Downstream influence of mesoscale convective systems: part 1, influence on forecast evolution

Article

Accepted Version

ORIGINAL ARTICLE

Downstream influence of Mesoscale Convective Systems: Part 1, influence on forecast evolution

S. J. Clarke[1] | S. L. Gray[1] | N. M. Roberts[2]

[1]Department of Meteorology, University of Reading, UK

[2]MetOffice@Reading, Reading, UK

Correspondence
S. J. Clarke, School of Earth and Environment, University of Leeds, Leeds, LS2 9JT, UK
Email: s.j.clarke@leeds.ac.uk

Funding information
Natural Environmental Research Council PhD studentship, Award reference: NE/I510110, with Met Office CASE award

Mesoscale convective systems (MCS) are difficult to forecast due to their inherent unpredictability and development from scales that are sub grid in typical global models. Here the impacts of model representation of convection on MCS structure and downstream forecast evolution are examined using two configurations of the Met Office Unified Model: the convection-permitting (4.4-km grid spacing) limited area Euro4 and convection-parametrizing (25-km grid spacing) Global configurations.

MCSs are associated with a characteristic potential vorticity (PV) structure: a positive PV anomaly in the mid troposphere and negative PV anomalies above and to the side of it. Convection-permitting models produce larger amplitude MCS PV anomalies than convection-parametrizing models. These differences are shown to persist after coarse graining the output from a Euro4 simulation to the 25-km grid spacing of the Global configuration for a case study from July 2012, and are largest in magnitude and extent in the upper troposphere.

The effect of the poor representation of this PV structure by convection-parametrizing models on forecasts is investigated by adding 'MCS perturbations', calculated as differences between the coarse-grained Euro4 and the Global outputs, to five-day Global configuration forecasts. Upper-level MCS perturbations lead to greater forecast differences than those at middle levels, though using perturbations at all

levels yields the greatest impact. For the first 36 hours differences grow on the convective scale related to the MCS and its influence on a developing UK cyclone, despite perturbation amplitudes initially reducing. Subsequently, differences grow rapidly onto the synoptic scale and by five days impact the entire northern hemisphere. MCS perturbations slow the eastward movement of Rossby waves due to ridge amplification. Thus, perturbing convection-parametrizing models to include PV anomalies associated with MCSs produces synoptic-scale forecast differences implying that the misrepresentation of the PV structures associated with MCSs are a potential source of forecast errors.

KEYWORDS
potential vorticity, convection-permitting, forecast error, convection, forecast bust, Met Office Unified Model, MCS

1 | INTRODUCTION

Houze (2004) defines mesoscale convective systems (MCS) broadly as cumulonimbus cloud systems that produce a contiguous precipitation area $\sim$ 100 km or more in at least one direction. They form as an amalgamation or organisation of individual thunderstorms into a single cloud system and occur most frequently in Africa, Australia, China, South America and the United States, although they are known to occur over the whole globe except for the Antarctic (Liang and Fritsch, 2000). They are relatively rare in the UK and Europe. The climatology of UK MCSs by Gray and Marshall (1998) (later extended by Lewis and Gray (2010)) showed that on average about two MCSs occur each year in the UK, typically during May to August. If they initiate over the UK then this usually occurs in the late afternoon and early evening, but UK MCSs are more likely to have initiated non-locally and then be advected over the UK. MCSs are often associated with extreme weather such as heavy and persistent rain, large hail, strong winds and occasionally tornadoes (Houze, 2004). In this study we use a case study of MCSs occurring in the UK and France and examine their influence on downstream forecast evolution. This choice of case study is motivated by MCSs occurring here being less well studied compared to MCSs elsewhere (due to their rarity) and the inherent unpredictability of MCSs having led to poor forecasts (Clark et al., 2016). Availability of an operational convection-permitting model configuration covering this region of MCS initiation and development also influenced our choice.

Numerical weather prediction (NWP) models have difficulties representing MCSs due to their evolution from individual thunderstorms (Wandishin et al., 2008, 2010). For grid boxes of about 10 km or larger, convection needs to be parametrized. Parametrization of convection assumes that an ensemble of clouds exists within each grid box, therefore this assumption breaks down for mature MCSs, due to their scale, which can potentially cause errors in model forecasts. Convection parametrization schemes are also steady state, i.e. they cannot represent the structural evolution of MCSs from individual thunderstorms, nor do they diagnose that an MCS is developing (rather than any other type of convection). At higher resolutions models can be run with the convection parametrization scheme turned off: these models are often termed convection-permitting models. A review of such models is presented in Clark et al. (2016) in

which they are defined as "models in which the dynamics of atmospheric convection is treated with sufficient accuracy in order to make it viable to switch off convection parametrization". However, computationally-expensive convection-permitting forecasts are often performed using limited area model configurations and so require lateral boundary conditions, usually provided operationally by a global model forecast. This requirement can limit the predictability of MCSs, especially when an MCS is advected into the domain of the limited area model after being initiated outside. Morris (1986) was the first to demonstrate that NWP models can accurately forecast the 'Spanish plume' synoptic environment typically associated with MCS development in western Europe (later followed by Young, 1995). However, while good convection-permitting forecasts of the magnitude and location of precipitation associated with MCSs are possible (Clark et al., 2014, 2016), accurate forecasting remains challenging.

The structure of MCSs can be usefully characterised using potential vorticity (PV), a conserved variable in the absence of diabatic and frictional processes. MCSs have an associated positive PV anomaly at middle levels that typically extends throughout most of the troposphere and a negative PV anomaly at upper levels (tropopause level) in the stratiform region of the MCS (Houze (2004) and references therein). These PV anomalies are generated by steady state mid-tropospheric heating, typically associated with the coherent updraughts found in MCSs, and are represented differently in NWP models with parametrized and explicit convection. For example, for simulations of two MCS case studies with three different partitionings between parametrized and explicit convection (all with 12-km grid spacing), Done et al. (2006) found that lenses of negative PV developed near the tropopause level when convection was represented explicitly (in addition to vertically-orientated positive and negative mid-tropospheric PV anomalies) that were not present when convection was parametrized. Convection was proven to lead to an anticyclonic circulation at upper levels by removal (in one of the cases) of the background flow generated in the absence of convection. Figure 11(c) of Done et al. (2006) shows vertically-orientated negative PV anomalies (of a few PVU) exist to the side of the mid-tropospheric positive PV anomaly. Stronger horizontal variations in PV have been found in higher-resolution convection-permitting NWP simulations. For a case of heavy showers Chagnon and Gray (2009) found that a convection-permitting simulation (1-km grid spacing) of deep convection produced deeper and more intense PV anomalies (on the order 10 PVU) than a corresponding convection-parametrizing simulation (12-km grid spacing; on the order 1 PVU). The convection-permitting simulation also produced horizontally-tilted dipoles of PV that were not produced in the coarser-resolution simulation. These horizontally-tilted dipoles are cumulus-scale PV anomalies that develop in a sheared environment and which cannot be developed by the convection scheme. Weijenborg et al. (2017) demonstrated that horizontal PV dipoles with statistically significant flow anomalies are consistently associated with convection by averaging over several thousand convective cells. They also showed that these PV dipoles have a longer lifetime than their associated convection and so may go on to influence flow evolution. Although small in scale and with a tendency to exist as coupled positive and negative anomalies, the deeper and more intense PV anomalies produced in convection-permitting (compared to convection-parametrizing) simulations may persist after being averaged onto the same grid scale as the convection-parametrizing simulations and so affect synoptic-scale error growth as discussed by Chagnon and Gray (2009).

Although MCSs only cover a mesoscale area, the convection, and associated latent heating and cooling mean that MCSs are an important link between atmospheric convection and the larger-scale atmospheric circulation (Houze, 2004). MCSs over North America have been linked to Rossby wave modification and subsequent forecast busts over Europe six days after their occurrence (Rodwell et al., 2013). Hence, the absence or misrepresentation of PV anomalies at near-tropopause levels associated with MCSs in convection-parametrizing simulations could similarly impact on the forecast downstream from the MCS as well as have an impact on the forecast of the MCS itself. Gray (2001) found that adding idealised MCS positive PV structures into NWP models (in convection-parametrizing simulations) in some cases caused a deepening of synoptic-scale disturbances downstream from the MCS itself. Sensitivity studies determined

that the mid-level positive PV anomaly with its associated areas of ascent and descent (rather than the upper-level negative PV anomaly) was the dominant influence on the downstream flow in these experiments.

MCSs are not the only intensely-convective weather events that impact Rossby wave structure and have been associated with reduced medium-range forecast predictability and skill — many studies have examined the impact of tropical cyclones undergoing extratropical transition. Keller et al. (2019) presents a review of these studies and reasons for the reduced forecast predictability. The direct impact of the transitioning tropical cyclone on the mid-latitude flow is described as the formation of a jet streak through advection of the negative PV anomaly by the divergent outflow, and amplification of a downstream ridge. Rodwell et al. (2013) similarly found North American MCSs to be associated with strengthening of a ridge positioned above the region with large CAPE values (on its northeast side). Grams and Archambault (2016) diagnosed three separate weather systems associated with transitioning tropical cyclones that contribute to the divergent outflow: preconditioning by a predecessor rain event; interaction between the tropical cyclone and extratropical flow; and a downstream warm conveyor belt. Other work has focussed on the importance of diabatic processes in extratropical cyclones for forecast error. For example, Martínez-Alvarado et al. (2016) linked errors in an operational forecast of a Rossby wave to errors in the forecast of a warm conveyor belt. Chagnon et al. (2013) and Chagnon and Gray (2015) demonstrated for a total of four cases studies that the warm conveyor belt outflow leads to little direct modification of the tropopause structure (in contrast to outflows from tropical cyclones and MCSs); instead the downstream influence is likely to arise from enhancement of the PV gradient across the tropopause and an associated enhancement of the upper-level jet. Harvey et al. (2016) showed that such faster jet speeds lead to faster Rossby wave phase speeds despite the increased ability of the waves to propagate upstream. Teubler and Riemer (2016) separately diagnosed the impact of upper-tropospheric divergent outflow (assumed to be mainly an "indirect" effect of latent heating below) and "direct" diabatic processes on Rossby wave evolution and found that the indirect effect dominates and, together with baroclinic growth, is particularly important in ridge building (for which the latent heating occurs in a warm conveyor belt). A seasonal analysis of the bust events identified by Rodwell et al. (2013) performed by Lillo and Parsons (2017) linked the bust cases to all of the weather systems discussed above: a peak in bust frequency in September–October was linked to recurving tropical storms in the central Atlantic, and June–July and January–February peaks were linked to North American MCSs and East coast cyclogenesis respectively.

The aim of this study is thus to investigate the possible impacts of poor representation of MCSs on global model forecasts with parametrized convection. More specifically, we investigate whether forecast (rather than idealised as in Gray (2001)) MCS PV anomalies in a convection-permitting model lead to impacts downstream from MCSs in lower-resolution model that can't represent convection explicitly. A case study from July 2012 is chosen as a typical example of European MCSs and which included a MCS that tracked over the UK. It is shown for this case study that the PV structure associated with the UK-tracking MCS in convection-permitting model output is more intense, even after coarse graining (i.e. averaging higher-resolution output onto a lower-resolution grid) to the resolution of a convection-parametrizing model, than the equivalent PV structure in the output of that convection-parametrizing model. Derived 'MCS perturbations' are then added to the convection-parametrizing model to determine the impact on the forecast evolution. The impact of these perturbations on ensemble forecast skill and spread are investigated for the same case study in the companion paper (Clarke et al., 2019).

An overview of the case study is given in Sec. 2. The numerical model and configurations used, coarse-graining procedure, generation of the MCS perturbations and root mean square difference diagnostic used to compare the simulations are described in Sec. 3. The PV structures of the MCSs in the convection-permitting and -parametrizing model configurations are contrasted in Sec. 4. In Sec. 5 the impact of MCS perturbations on the convection-parametrizing forecast are demonstrated. The dependence of this impact on the positive mid-tropospheric and negative upper-tropospheric PV anomalies separately and on the perturbation magnitude are explored in Sec. 6. Finally, Sec.7 contains

the conclusions.

2 | OVERVIEW OF THE MCS CASE STUDY: 5–6 JULY 2012

Prior to the development of the MCSs a cut-off low-pressure system to the west of the UK was almost stationary for four days in association with an area of blocking high pressure to the east of the UK over Scandinavia. This allowed favourable conditions for deep, organised convection to form. Warm, moist air from over the North Atlantic flowed inland over the Iberian Peninsula and then turned north-eastwards towards France and the UK. A cold front running through the centre of France had a weak upper-level trough associated with it (marked on Fig. 1(a)). This frontal temperature gradient and weak upper-level trough created the necessary triggering mechanism for the deep convection in this case through the vertical motion forced by the upper-level positive vorticity advection. Convection initiated around 00 UTC on 5 July in southern France (Fig. 1(d) shows the satellite imagery at 0230 UTC). Further triggering occurred at 09 UTC and the resultant organised MCS (hereafter MCS-A) reached maturity at 18 UTC as it tracked northwards towards the UK (comparison of Figs. 1(b) and (e) shows the MCS lying along a marked cold front at this time). The rainfall radar (not shown) shows a region of precipitation that grows in size and intensifies (to rates exceeding 10 mm h^{-1}) during 5 July; this region was associated with an increasing number of lightning reports covering an area large enough to satisfy the MCS criteria (not shown). A large surrounding stratiform area generating 1–2 mm h^{-1} of precipitation also existed. After 21 UTC this MCS began to decay and interacted with a developing frontal cyclone over the UK (Fig. 1(c) and (f)). A second MCS (hereafter MCS-B) formed over the south of France at 18 UTC (Fig. 1(e)) and was also associated with a large number of lightning reports and heavy precipitation exceeding 10 mm h^{-1} (not shown). This second MCS tracked eastwards towards Italy and Germany and dissipated by 12 UTC 6 July (the time of Figs. 1(c) and (f)).

The synoptic environment in which the MCSs formed is consistent with the modified Spanish Plume environment identified by Lewis and Gray (2010) from a climatology of MCSs that affected the UK. They described this environment as associated with "a slowly moving mature frontal system associated with a forward tilting trough (and possibly cut-off low) at 500 hPa that evolves according to idealised baroclinic life cycle 2" (where the baroclinic lifecycles are as described by Thorncroft et al. (1993)). Conditional instability is released from a warm moist plume of air advected northeastwards from Iberia that is capped by warmer, but very dry well-mixed air, from the Spanish plateau. Analysis of convective available convective energy (CAPE) for this case study using analyses from the, then operational, North Atlantic European configuration of the Met Office Unified model (MetUM) with approximately 12-km grid spacing (not shown) reveals that CAPE values were 1000–1600 J kg^{-1} where MCS-A began to develop at 00 UTC 5 July. However, considerable convective inhibition limited convection from instability release from the lower troposphere. By 09 UTC, when MCS-A organised, CAPE values were around 1800 J kg^{-1} and in the absence of convective inhibition convection initiated from near the ground; this CAPE value reduced to around 800 J kg^{-1} by 12 UTC.

3 | MET OFFICE UNIFIED MODEL

3.1 | Model and configurations used

Version 8.2 of the MetUM has been used for this study. This version used the so-called "New Dynamics" dynamical core (Davies et al., 2005) that was operational in 2012. The MetUM solves nonhydrostatic, deep-atmosphere dynamics using a semi-implicit, semi-Lagrangian numerical scheme. The grid has Arakawa C staggering in the horizontal and a terrain-following hybrid height vertical coordinate with Charney-Philips staggering. We use two configurations of

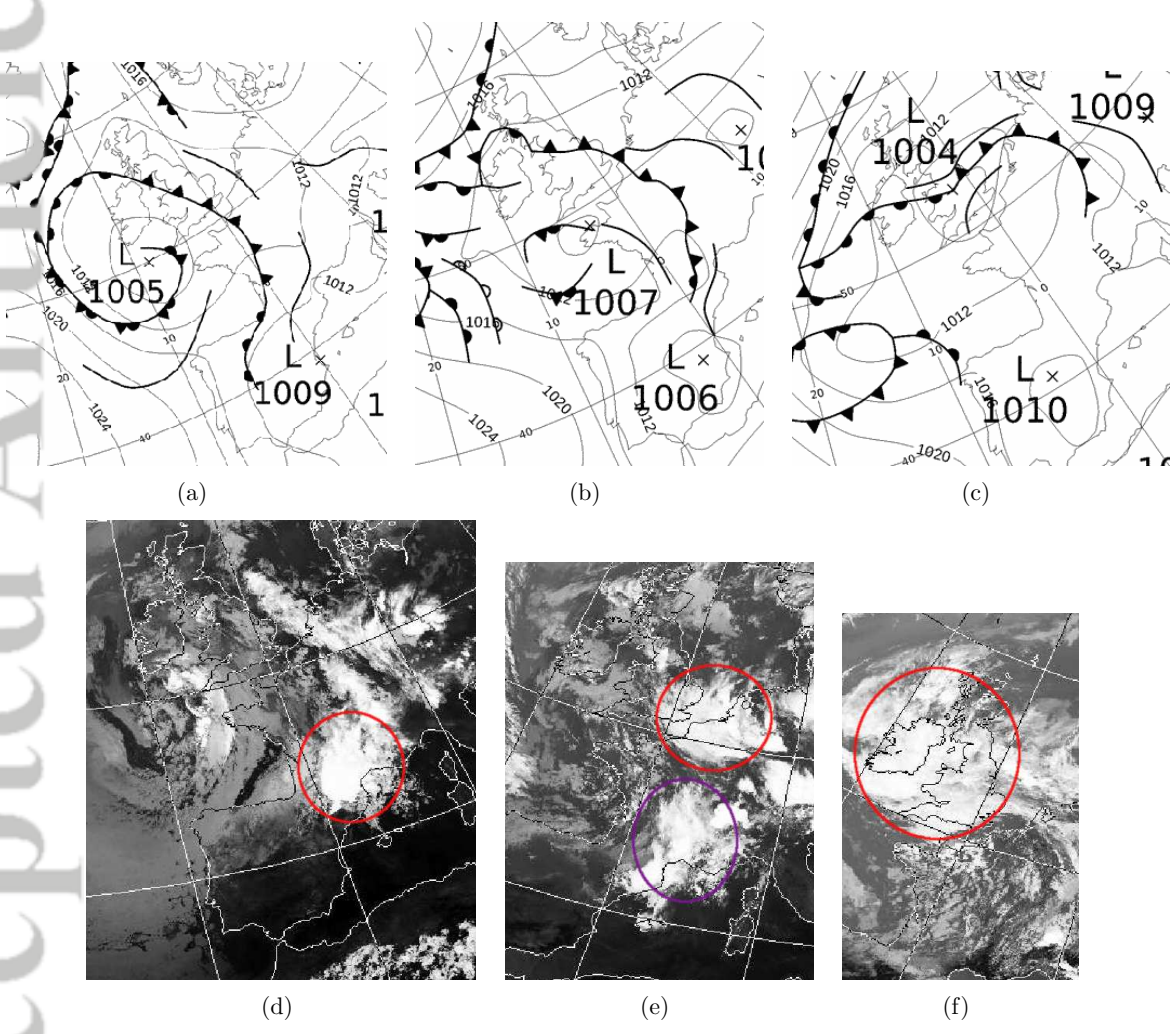

FIGURE 1 Met Office synoptic analysis charts for (a) 00 UTC 5 July, (b) 18 UTC 5 July, and (c) 12 UTC 6 July 2012 (Archived by www.wetter3.de, Crown copyright) and infra-red satellite images for (d) 0230 UTC 5 July, (e) 1936 UTC 5 July and (f) 1214 UTC 6 July 2012 (Courtesy of Dundee satellite receiving station). The red and purple ellipses in the satellite imagery mark the locations of MCS-A (red) and MCS-B (purple), respectively, discussed in the text.

the MetUM that were operational (with the chosen grid spacings) at the time of the 2012 case study. The first is a convection-permitting model configuration, the so-called "Euro4" configuration which has a 4.4-km horizontal grid spacing with a domain covering much of Europe and extending to the North Atlantic on a rotated latitude-longitude grid. It has 70 vertical levels and a lid at 40 km. This configuration was chosen because it was the only operational convection-permitting configuration that includes the region of initiation of the two MCSs within its domain. The second configuration is a global convection-parametrizing configuration that has 25-km horizontal grid spacing (hereafter Global configuration). It also has 70 vertical levels, but extending to a lid at 80 km. The Global configuration is termed "convection-parametrizing" because a convective parametrization scheme is required to deal with convection that is not explicitly represented on such a coarse horizontal grid.

Each model uses a set of parametrizations including (but not limited to) those for the boundary layer (Lock et al., 2000), cloud microphysics (Wilson and Ballard, 1999), and convection (Gregory and Rowntree, 1990). For the Euro4 configuration the grid spacing is fine enough for convection to be explicitly represented. However, the resolution is in the "grey" zone in which many showers are only partially resolved (and cloud sub-structure is still completely unresolved). This partial resolution means there is still a need to parametrize the smaller showers, but if the convection parametrization scheme is used as configured for the Global configuration it will effectively remove convective instability before any explicitly-represented convection can develop. To try to combat this problem the Euro4 configuration uses a version of the Gregory and Rowntree (1990) convection parametrization scheme that has been modified to limit its activity (Roberts, 2003). This modification, although not a complete solution (and much work is now being done in this area e.g. Arakawa et al. (2016)), does improve the representation of convection on the ~4-km grid. Nevertheless, there are still issues at this grey-zone resolution: showers are typically too sparse, too intense and initiate too late (Lean et al., 2008; Clark et al., 2016). The problems are much reduced when simulating larger, better-resolved convective systems like the MCSs studied here and therefore we argue that the resolution is sufficiently fine for the purposes of this work, although with caveats discussed later. The Euro4 simulations use boundary and initial conditions from the Global configuration simulation; the Global configuration simulation starts with initial conditions from the Met Office operational analyses. The Global configuration simulation was initiated at 00 UTC 5 July and run out to 18 UTC 5 July. Fields were output at 03 UTC from which the downscaled Euro4 simulation was initiated. The Euro4 simulation was then also run out to 18 UTC 5 July. This setup is shown schematically on the left-hand-side of Fig. 2.

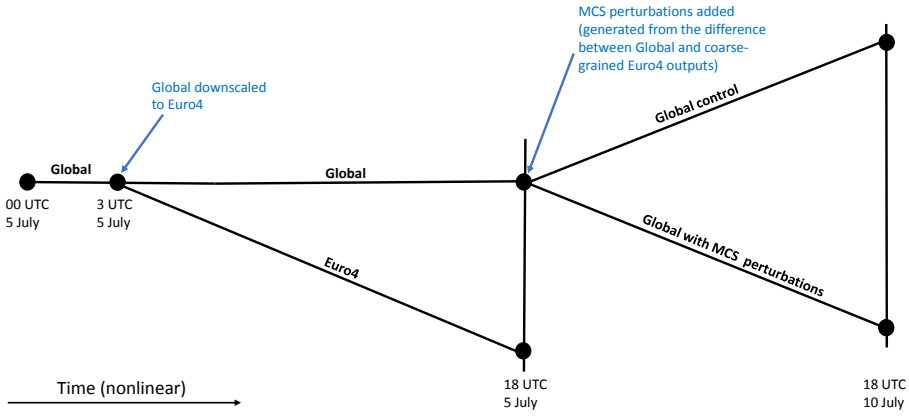

FIGURE 2 Schematic illustrating the generation of the two corresponding Global configuration forecasts with and without MCS perturbations.

3.2 | Coarse-graining procedure

To compare the outputs from the Euro4 and Global configurations of the model, they must be at the same resolution and on the same model grid. Hence the outputs need to be coarse grained to a resolution that is at least as coarse as that used in the Global configuration (if the comparison coarse resolution is that of the Global configuration then only the Euro4 output needs coarse graining). The coarse graining is performed by averaging the output to the required coarse resolution. To do this the new model grid points are defined and averaging performed. A complication arises because the Euro4 configuration uses a rotated latitude-longitude grid, unlike the Global configuration. Consequently, the model output is first interpolated onto an un-rotated model grid that is of higher resolution than that of the Euro4 output (specifically twice the resolution). The required subdomain (the region where the perturbations are calculated) of this interpolated output is then averaged onto an un-rotated model grid with the required coarse resolution.

3.3 | Perturbation insertion method

Wind and temperature perturbations associated with the MCSs are calculated by taking differences between corresponding Global and Euro4 configuration simulations once the Euro4 has been reconfigured to the Global grid. It is assumed that the differences between the simulations are dominated by the explicit representation of the MCSs in the Euro4, but not the Global, simulation. However, differences may have also evolved due to other processes within the Euro4 during the 15 h after the Global simulation was downscaled to the Euro4 resolution (although the use of boundary conditions from the Global simulation will have helped to constrain the Euro4 evolution and the fastest-acting mesoscale process through the depth of the troposphere is nevertheless the development of the organised deep convection and MCSs). Figure 2 shows that the perturbations are added 18 h into the Global configuration simulation at 18 UTC 5 July, which is when the MCSs in the Euro4 simulation have become mature. The variables used are the zonal (u) and meridional (v) components of wind, and potential temperature (θ). These act as a surrogate for the PV which is the diagnostic we use to analyse the MCS structure, but is not a MetUM prognostic variable. Unlike in previous studies where balanced perturbation structures have been diagnosed through PV inversion (e.g. Gray (2001) used a Charney non-linear balance technique to calculate wind and θ perturbations for his idealised MCSs), the perturbations applied here are not designed to satisfy any particular balance constraint. Instead, they are coherent structures that represent the rapidly-developing convection. As noted by Weijenborg et al. (2017), associated PV structures can be coherent even though deep moist convection is very unsteady and so it is unlikely that the flow around the mesoscale dipoles meets synoptic-scale balance constraints such as thermal wind balance. As a further argument for not imposing balance we show in Sec. 4 that the developing MCSs are associated with coherent regions of negative PV: negative PV cannot be inverted and indeed Gray (2001) assumed a very small positive value for the upper-tropospheric PV anomaly to enable inversion rather than a negative value, as is characteristically associated with MCSs (see Sec. 1). Finally, we note that it is not thought problematic in national Met Services to insert "random parameter" perturbations into an ensemble to take account of "model error" and these are almost certainly not balanced (e.g. see Bowler et al. (2008) and McCabe et al. (2016) for a description of the random parameter scheme used by the Met Office global and convection-permitting ensembles, respectively).

The perturbations are calculated over a limited area covering the region of western Europe affected by the two MCSs (approximately 40–54°N, 7°W–8°E). Four types of MCS perturbations are introduced:

1. ALLPERTS: perturbations added over all model levels.
2. UPERTS: perturbations added at the levels around the tropopause only (levels 33–40; approximately 250–350 hPa).

These levels were chosen because they showed the largest magnitude differences between the Euro4 and Global simulation outputs after coarse graining.

3. MPERTS: perturbations added at mid-tropospheric levels (levels 18–30; approximately 450–750 hPa). These levels are where the positive PV towers associated with the MCSs are most prominent in the Euro4 simulation output.
4. X3PERTS: UPERTS perturbations multiplied by a factor of three. These perturbations are used to see if stronger perturbations at upper levels have a greater impact on the downstream forecast evolution.

Figure 3 shows the θ and v perturbations at approximately 500 hPa (mid troposphere) and 250 hPa (jet-stream level). The perturbation magnitudes are larger at upper levels and have amplitudes of up to 8 K and 15 m s^{-1}, respectively. The θ perturbations are mostly positive at both levels as a result of the warming produced by the explicitly-represented MCSs in the Euro4 simulation. The warming is associated with increased mid-tropospheric PV and reduced upper-tropospheric (jet-stream level) PV as discussed later (Sec. 4). Figure 3(d) shows that the tropopause-level wind perturbations are large and are coherent over large scales, with divergence above the MCSs. The wind perturbations extend to the edges of the perturbation region, implying that the influence of the MCSs (or more precisely the difference between the Global and Euro4 simulations attributed primarily to the explicitly-represented MCSs in the Euro4 simulation) extends beyond the region over which the perturbations are inserted into the Global simulation. Hence, a larger perturbation region could have been reasonably considered; however, a larger region is more likely to include perturbations that are not mainly attributable to the identified MCSs.

The MCS perturbations are inserted into the Global simulation using the MetUM's incremental analysis update (IAU) scheme (Clayton, 2012). The IAU scheme allows increments to be added gradually over several timesteps with the fraction added at each timestep being determined by a (discrete) IAU weighting function (Bloom et al., 1996). The gradual insertion reduces the shock to the simulation and prevents some of the spurious noise that would otherwise be created, especially if the increments are large as is the case at tropopause level here. The increments were added uniformly over a 60-minute period at 10-minute intervals (the model timestep). The Global simulations were then run for 3 days starting at 18 UTC 5 July 2012 (the time at the start of the IAU perturbation insertion) for the four perturbation experiments (ALLPERTS, UPERTS, MPERTS, X3PERTS) and also with no perturbations added. The differences between the forecasts with and without the perturbations were then analysed. This simulation sequence is shown schematically

3.4 | Root mean squared difference (RMSD)

RMSD is used in this study as a measure of the differences, for a given output field, between a Global configuration forecast with MCS perturbations added and the Control forecast without the perturbations:

$$RMSD = \sqrt{\frac{\sum_1^N (x_i - y_i)^2}{N}},$$

where N is the number of points in the domain, x_i is the value of the field (at point i) in the forecast with the MCS perturbations added and y_i is the value of the field from the Control forecast without the perturbations.

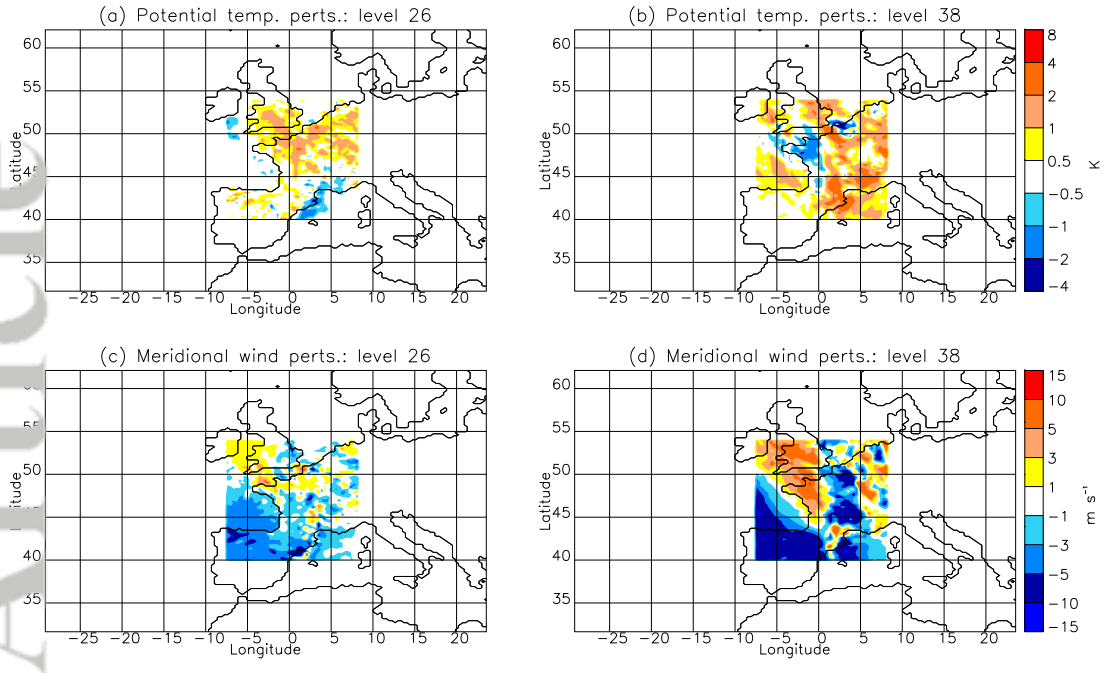

FIGURE 3 MCS ALLPERTS perturbations for θ at model levels (a) 26 (approximately 500 hPa) and (b) 38 (approximately 250 hPa), and for meridional windspeed at model levels (c) 26 and (d) 38.

4 | DEPENDENCE OF MCS STRUCTURE ON MODEL RESOLUTION

Convection-permitting model simulations can explicitly represent localised convection on a fine grid, whereas convection-parametrizing simulations only represent an average effect of unresolved convection (e.g. Clark et al., 2016). This explicit representation of individual convective updraughts leads to stronger associated negative and positive PV anomalies along with a finer-scale PV structure (Done et al., 2006). It is not obvious whether these differences still exist when the output from such simulations are smoothed to the same resolution since positive and negative PV anomalies tend to be coupled. To determine this, the output from the Euro4 simulation was coarse grained to the grid spacing of the Global configuration and compared with the Global output. Here, and in the following section, we focus on the 250-hPa PV and geopotential height fields (hereafter PV250 and Z250, respectively) as we hypothesize that tropopause-level PV differences are most likely to impact downstream flow evolution. We also show surface precipitation rates to relate the precipitation to the PV structures and so give the context of where the MCSs occur.

Figure 4 shows precipitation rates, PV250 and Z250 at the time of organisation of MCS-A in the output from the Global and Euro4 configuration simulations. Both model configurations produce precipitation in the approximate location of the observed MCS (compare Fig. 4(a, b) to the satellite image in Fig. 1(d), though note that the satellite image is from a few hours earlier). As is typical, the precipitation rates field in the Global configuration output has a smoother, broader structure and smaller magnitudes than that in the Euro4 configuration output (precipitation rates are up to 30 mm h^{-1} in the Euro4 output compared to 8 mm h^{-1} in the Global output). The PV250 fields (Fig. 4(c, d)) show stratospheric air (PV values exceeding 3 PVU) in the west of the domain shown associated with the large-scale upper-level trough that is also indicated by the low Z250 values. In the Global configuration output there is no obvious

signature of MCS-A in PV250. In contrast, in the Euro4 output this MCS is associated with a noisy field of anomalous PV250 over eastern France (at about 47°N, 4°E), with negative PV values as low as -6 PVU in the core of the region surrounded by positive values of up to 12 PVU. For comparison, a similar noisy upper-tropospheric (350-K isentropic surface) PV structure, dominated by negative values with magnitudes up to about 10 PVU, is shown in Fig. 16(b) of Shutts (2017) for an MCS case study simulated using the MetUM with 2.2-km grid spacing. There are likely two contributors to the lack of a strong PV signature at this level over southwest France (where there is heavier precipitation) at this time. First, it is well established that the cyclonic circulation (and thus associated PV anomalies) develops within the trailing stratiform precipitation region of MCSs (e.g. see Fig. 21 in the review article by Houze (2004)): the noisy PV field (which is predominantly negative PV anomalies) is associated with the stratiform region of the MCS, where there is lighter precipitation. To the northwest of this stratiform region is an area of heavy precipitation associated with the leading convective region of the northwestwards-moving MCS. Second, since the PV anomaly structure is a consequence of the integrated effect of the latent heating, the weaker (relative to that in eastern France) earlier convection in southwest France will have led to a weaker PV signature there than might be anticipated from the instantaneous precipitation field shown in Fig. 4(b).

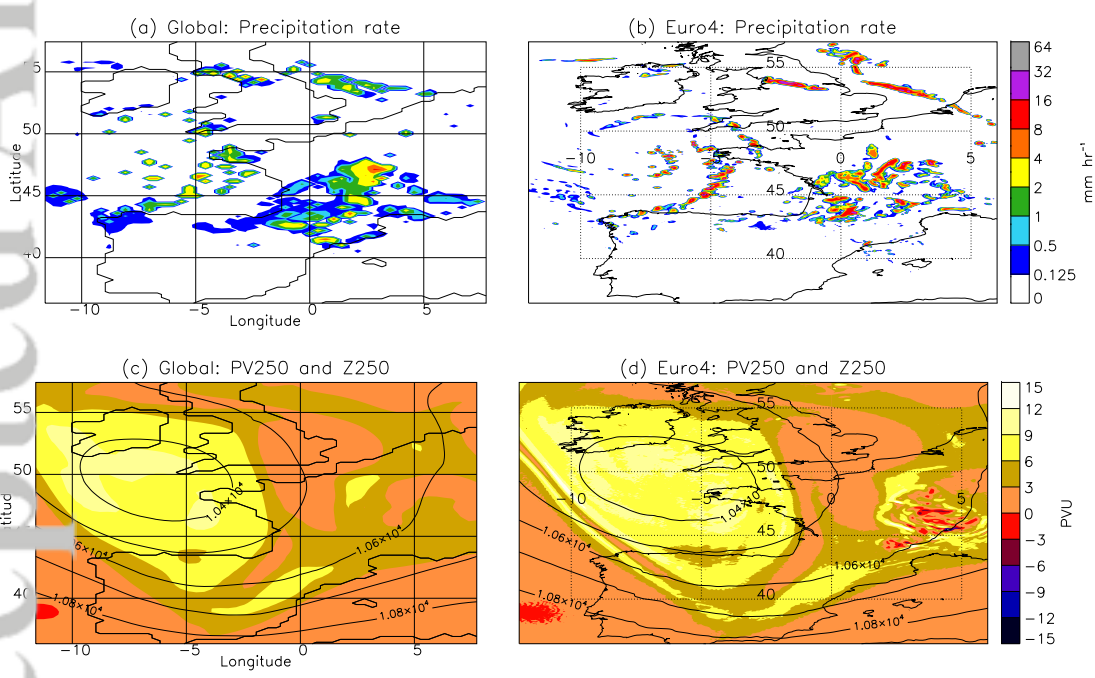

FIGURE 4 (a,b) Total precipitation rate for (a) the Global, and (b) the Euro4 configuration simulation output at 09 UTC 5 July 2012; (b,c) as for (a,b) but for PV250 (in PVU, shaded) and Z250 (in m, contours).

Figure 5 shows precipitation rates and PV250 from both configurations 12 h later when MCS-A (on the Belgium coast at about 51°N, 4°E) has become a mature systems and MCS-B (located on the border between France and Spain at about 43°N, 3°E) has also developed strongly. The precipitation rates show that although the Global configuration initiated MCS-A, it did not maintain its development and by this time there is barely any associated precipitation. In contrast, MCS-A has been maintained in the Euro4 simulation and can be seen in approximately the observed location (compare Fig. 5(b) to the satellite image in Fig. 1(e)). MCS-B is represented in the output from both configurations.

Again the precipitation rates are lower and have a smoother structure in the Global configuration output. At both this and the earlier time the precipitation rates in the Euro4 configuration output are more intense than was observed by radar (not shown), consistent with the previously discussed characteristics of this model configuration (Sec. 3.1). The larger-scale upper-level trough (and associated region of large PV values) present 12 hours earlier (Fig. 4(c, d)) has now elongated and stretches across Ireland, through France, to the Mediterranean in the domain shown (Fig. 5(c, d)). The location of the upper-level trough remains very similar in the two simulations although small differences exist associated with the synoptic-scale impact of the MCSs. The MCSs are located on the northern flank of this region with large PV values. The PV signature associated with the two MCSs in the Euro4 output is seen as a wide area of noisy, but mainly negative, PV values with detailed fine-scale structure: negative values exceed a magnitude of 6 PVU in small regions. The Global configuration simulation fails to develop MCS-A and hence an associated PV signature is not seen. However, a small region of negative PV values (at about 45°N, 3°E) is associated with MCS-B. MCS-B appears to have led to a marked narrowing of the south-eastern tip of the larger-scale region of large PV values in the Global simulation and a destruction of the large PV values at the south-eastern end of the trough in the Euro4 simulation.

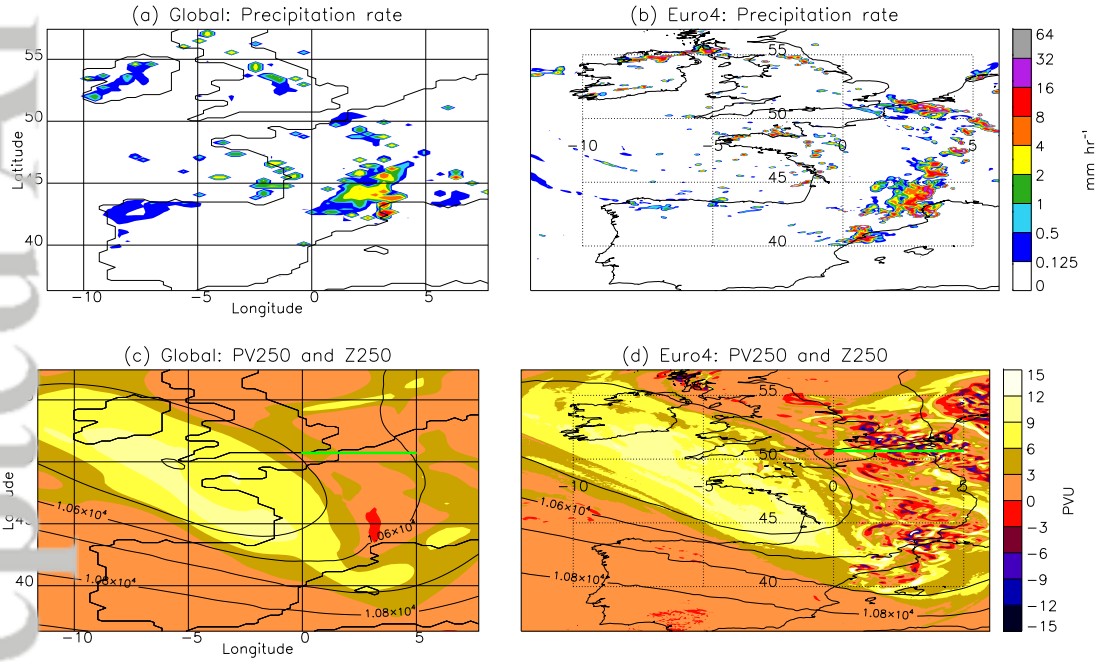

FIGURE 5 As for Fig. 4, but for 18 UTC 5 July 2012. The green lines in panels (c) and (d) indicate the cross-sections shown in Fig. 6. Note that PV250 values less than -15 PVU exist in isolated grid boxes in (d).

Figure 6 shows west–east vertical cross-sections though MCS-A at 18 UTC from both configurations. Looking first at the Global configuration output (Fig. 6(a)), we see that there is a region of slightly stronger PV (>0.8 PVU) in the cloudy mid-troposphere between 650 and 400 hPa (overlain relative humidity contours at 80 and 90% indicate cloudy regions). This weak PV anomaly and the presence of a lower-tropospheric dry layer (700–800 hPa) are consistent with there being little precipitation at this time (Fig. 5(a)). The cross-section through the Euro4 output (Fig. 6(b)) is markedly different. It consists of two vertically-extending mid-tropospheric positive PV anomalies (centred at about 550 hPa) with PV magnitudes exceeding 6 PVU flanked by negative PV regions extending from 900–200 hPa. The

air is cloudy where the strong PV anomalies exist. This PV structure resembles that shown in Fig. 11(c) of Done et al. (2006) (from output of a 12-km grid spacing version of the MetUM run with fully-explicit convection), although in that paper there is only one positive PV anomaly. Chagnon and Gray (2009) showed theoretically and using idealised numerical experiments how horizontally-orientated PV dipoles are generated when cumulus storm-induced heating is on a sufficiently small scale relative to the Rossby radius of deformation in the presence of moderate vertical windshear.

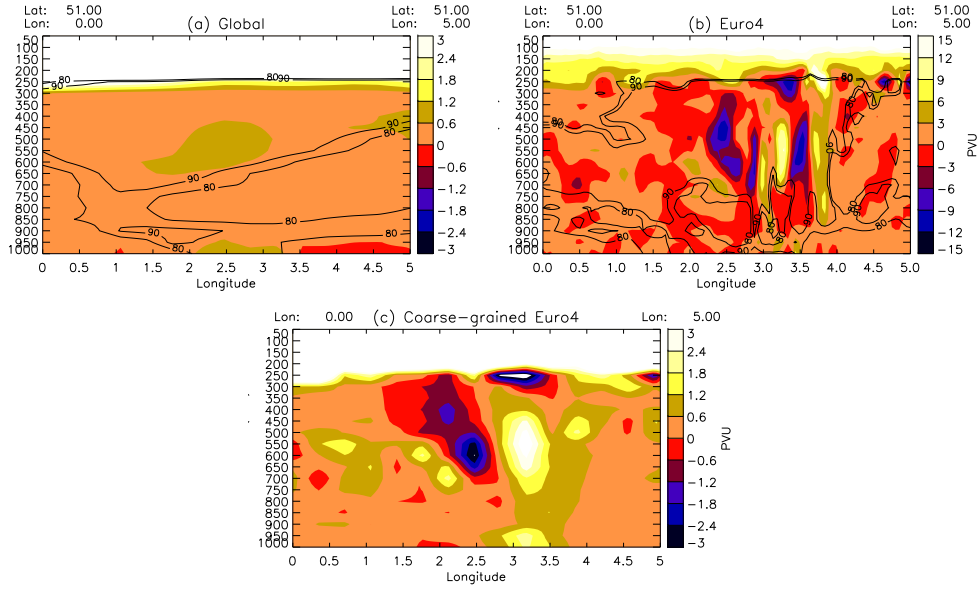

FIGURE 6 West–east vertical cross-section of PV through MCS-A at 18 UTC 5 July 2012 for (a) the Global output, (b) the Euro4 output and (c) the coarse-grained Euro4 output. Note that the colour scale in (c), selected to match that in (a), saturates as indicated by small white patches within blue and red regions; also, the colour scale in (b) has a range five times that of the scales for (a) and (c). Contours of relative humidity (at 80 and 90%) are overlain in (a) and (b) and the locations of the cross-sections are indicated on the maps in Figs. 5(c,d).

After coarse graining the Euro4 output loses some of its detail (Fig. 6(c)), but nevertheless retains a large coherent positive PV tower (at 3–3.5°E) with regions of negative PV to the east and above the tower at the tropopause level. Although the magnitudes of the PV anomalies are less in the Euro4 after coarse graining, they are still substantial (positive and negative values more than 3 PVU in magnitude) and considerably greater than in the Global output. Considering now the tropopause level (Fig. 7(a)), the coarse-grained Euro4 has negative PV areas where there was deep convection: PV values less than -6 PVU still exist in the region of MCS-A. Negative differences exceeding -1 PVU are found over a broad area (and exceeding -3 PVU in localised regions) in the regions of the observed MCSs when the Global output is subtracted from the coarse-grained Euro4 output (Fig. 7(b)). It is noticeable that the differences cover a wide area and therefore we may expect that they reflect large-scale differences in the tropopause-level flow too. This wide area implies that it would not have been unreasonable to have chosen to insert the MCS perturbations over a larger area, likely leading to enhanced impact (as also discussed in Sec. 3.3).

The effective resolution of a gridded numerical model is typically considered to be four to six times its grid spacing. Hence comparisons were also made between the Euro4 and Global outputs when both were coarse grained to a larger grid spacing than that of the Global model. The differences in PV structure associated with the MCS are retained even

when the outputs are coarse grained onto a grid with 100 km grid spacing (not shown). Negative values still exist at 250 hPa in the regions of the MCSs (magnitudes up to 1 PVU in the region of MCS-A) with negative differences with magnitudes of up to 4 PVU in these regions when the coarse-grained Global output is subtracted from that of the Euro4 output. However, whereas localised negative upper-tropospheric PV values associated with the MCS are retained in the Euro4 output after coarse graining to 100 km grid spacing, there is no clear positive or negative PV signature after coarse graining in the mid-troposphere because those anomalies are generated at smaller horizontal scales.

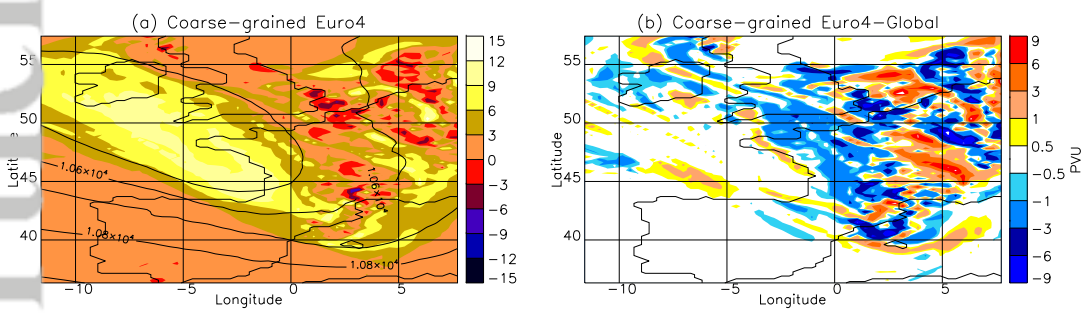

FIGURE 7 (a) PV250 (shaded) overlain with contours of Z250 for the coarse-grained Euro4 configuration simulation output and (b) difference between the coarse-grained Euro4 and Global configuration simulation PV250 outputs (note that the colour scale saturates as indicated by small white patches within blue and red regions). Both panels for 18 UTC 5 July 2012.

The persistence of the differences in the magnitudes of the PV structures associated with MCSs in the Euro4 and Global simulation outputs after coarse graining implies that the parametrization of convection lacks the ability to produce MCS structures that are nevertheless large enough to be represented on the Global configuration grid and so may have impacts on synoptic-scale downstream flow evolution. The hypothesis that poor representation of MCSs by convection-parametrizing models can impact synoptic-scale flow evolution is tested through the insertion of wind and θ of perturbations derived from these differences into Global configuration simulations in the next section.

5 | DOWNSTREAM INFLUENCE OF MCS PERTURBATIONS: FORECAST EVOLUTION

The impacts of the ALLPERTS perturbations (calculated as described in Section 3.3) on the Global forecast evolution are presented at three times: after 1 h (immediately after the perturbation insertion), after one day (between 00 and 18 UTC 6 July) to examine the impact on the developing cyclone, and then out towards medium range (up to five days, 10 July) to examine downstream development. Figure 8(a, c) shows the immediate impact of the perturbations on Z250 and PV250. The MCS perturbations lead to a dipole in Z250 change with a reduction exceeding 30 m along the axis of the upper-level trough that lies over the UK at this time (strongest at southwest of the trough's tip) and an enhancement to the southwest of this deepening exceeding 10 m. Hence the perturbations act to deepen the upper-level trough and also sharpen the horizontal gradient in Z250 on the western edge of the trough tip. There is also a small increase to the northeast of the trough (at about 52°N, 7°E). This change in Z is consistent with the deepening of the trough increasing the south-easterly jet streak on the eastern flank (not shown) as would be expected if the upper-level PV is largely reduced to the east because of the effect of the MCSs. Note that, as discussed in Sec. 3.3, as well as the impact of the MCSs at both local and synoptic scales, the perturbations also likely include other differences arising from the

evolution of the Euro4 forecast diverging somewhat from the Global forecast after 15 hours of running due to effects in the different model configurations. In this experiment we wanted to allow time for the convection to develop in the Euro4, hence 15 hours, but that does leave the opportunity for other differences to develop in the flow. Despite that, we are confident that the largest effect of the perturbations comes from the MCSs, especially because the perturbations were only added in a region local to the MCS cloud signatures. The impact of the perturbations on Z250 extends beyond the region of the impact on PV250 (compare (Fig. 8(c) and (a)); this difference is likely due to the property of PV known as action-at-a-distance (the influence of a PV anomaly on temperature and circulation extends spatially beyond the region of the PV anomaly, e.g. Thorpe and Bishop (1995)). The PV250 difference field arising from the perturbations is far noisier than that for Z250 and the region of large differences closely matches that used for insertion of the MCS perturbations (compare to Fig. 3). However, the differences are structurally-similar to the differences between the Euro4 and Global PV field at this level (compare to Fig. 7(b)) implying that the PV differences arising from the explicit representation of the MCSs in the Euro4 simulation have been reproduced by perturbing the Global simulation using the surrogate wind and θ differences. The strip of relatively weak negative perturbations on the western edge in the insertion region may again be to do with some evolution differences between the two simulations that are not directly related to the MCSs.

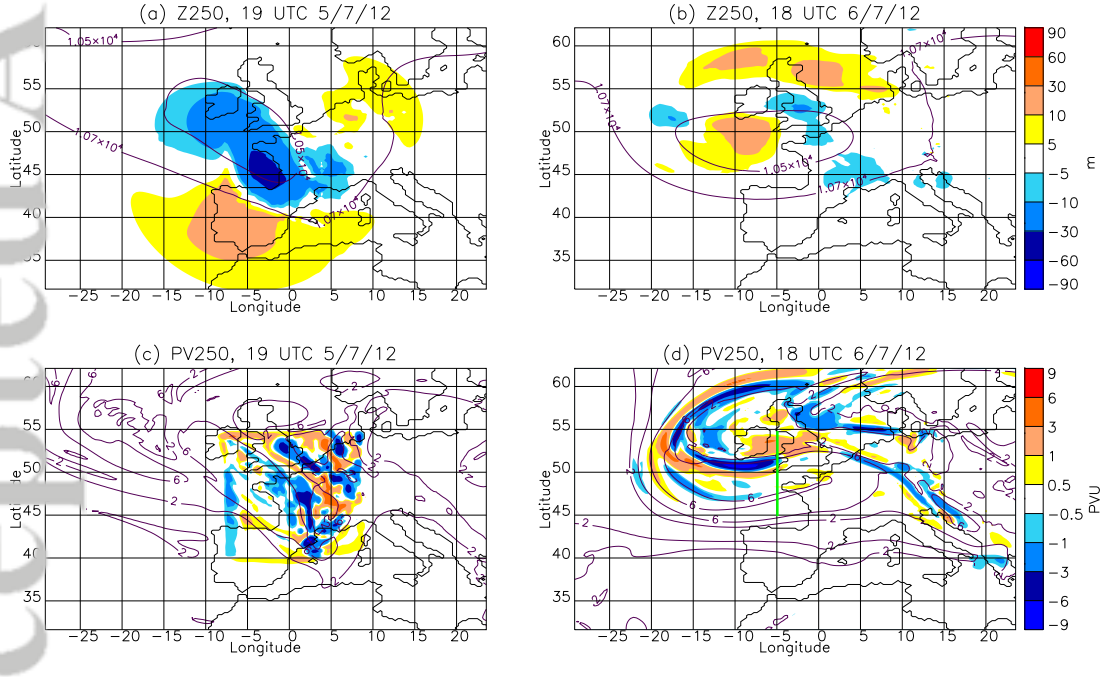

FIGURE 8 (a) Differences in Z250 (ALLPERTS minus Control) overlain with contours of Z250 (in m) from the Control simulation 1 h after the perturbations were inserted; (b) As for (a), but for 1 day after the perturbations were inserted; (c, d) As for (a,b) respectively, but for differences in PV250 overlain with contours of PV250 (in PVU) from the Control simulations. The green line in panel (d) indicates the cross-section shown in Fig. 10(a).

The impact of the MCS perturbations on the weak cyclone that developed over the UK on 6 July is now considered. This cyclone was associated with a broad region of cloud (Fig. 1(c, f)) and widespread precipitation (not shown). Figure 9 shows the precipitation rates in the Global configuration simulations with and without the MCS perturbations added.

At 00 UTC on 6 July the MCS perturbations have led to an intensification of MCS-A (located on the Belgium coast at about 52°N, 2°E) and intensified the precipitation in northeast France (at about 48°N, 4°E) that is largely missing in the simulation without the perturbations, but is seen in observations. The perturbations have also led to a deepening of the low pressure over northern France and the southern UK close to the MCSs (e.g. consider the 1008 and 1010 hPa pressure at mean sea level (PMSL) contour over southern England). This is a small effect at 00 UTC, but more apparent at 12 UTC 6 July, when the area enclosed by the 1006 hPa PMSL contour is greater with the MCS perturbations and hence the PMSL is closer to the analysed value there of 1004 hPa (Fig. 1(c)). The precipitation wrapping around the cyclone has a more curved structure at 12 UTC than at 00 UTC (compare Figs. 9(c) and (d)). Again this is closer to the observed pattern with the MCS perturbations added, especially on the western side and in the more northerly position of the line of precipitation associated with the fronts (compare to Fig. 1(c)). However, both simulations fail to capture the full extent of the UK precipitation which extends also over southeast England (not shown).

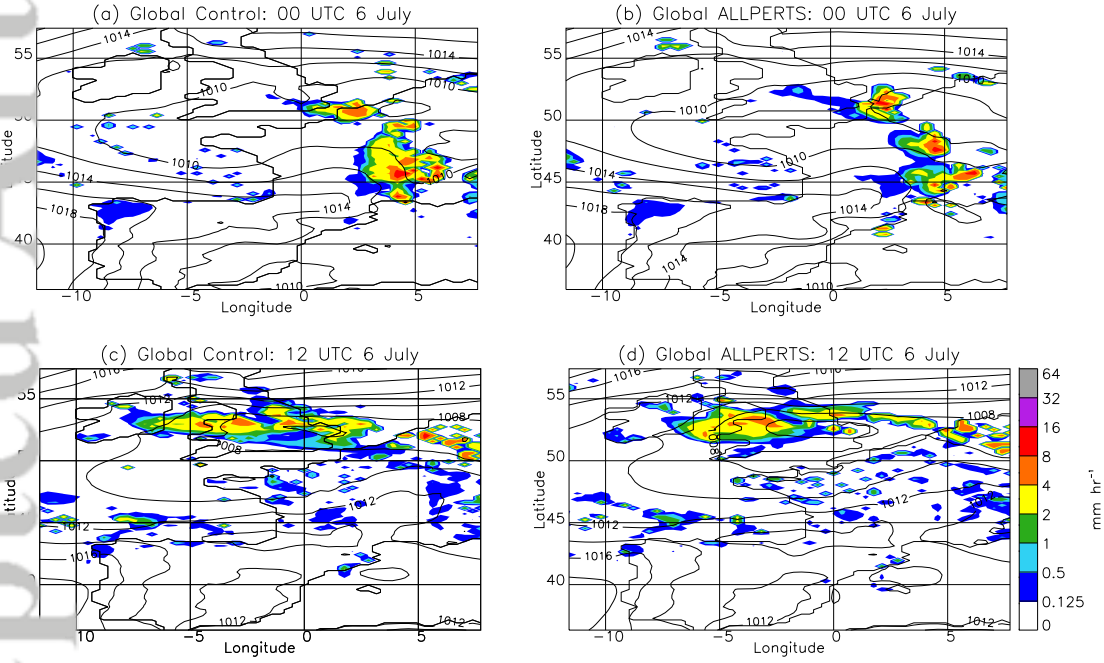

FIGURE 9 Total precipitation rates and PMSL (in hPa, contours) for (a, b) 6 h (00 UTC 6 July 2012) and (c, d) 18 gr (12 UTC 6 July 2012) after the MCS perturbations were inserted. (a, c) Control output and (b, d) output with ALLPERTS perturbations.

One day after the insertion of the perturbation, at 18 UTC 6 July, the Z250 differences are reduced compared to the immediate impact, particularly dramatically over Spain (Fig. 8(b)), but the PV250 differences (Fig. 8(d)) are retained with an extended coverage of filaments of increased and decreased PV wrapping around the upper-level trough that now hooks around the UK with its tip over France (see contours from the Control simulation in Figs. 8(b) and (d)). PV modification is focussed along the inner edge of the hooked PV filament with a negative band lying along the overlain 2-PVU contour (i.e. along the tropopause) and a positive band outside of this (in the air with larger PV values). The pattern of PV modification implies that the MCS perturbations have led to erosion of the inner edge of the PV filament and enhancement of the isobaric PV gradient here together with northwards shifting of the southern tip of the PV

filament (consistent with enhanced cyclonic curvature of the filament). The dipole in Z250 (positive pole south of Ireland and negative pole over England) leads to a more northeast-southwest tilted trough, consistent with the PV modifications. A vertical south–north cross-section taken through the frontal, tropopause-fold, region associated with the cyclone (Fig. 10(a)) shows a generally marked decrease in PV at the tropopause level in the frontal region (50–52°N), with some increase in PV to the south (at about 49°N). The MCS perturbations have essentially acted to shift the pattern at tropopause level towards the south and sharpened the fold leading to a horizontal dipole in PV modification (this shift in position of the tropopause was also found in Joos and Forbes (2016) when investigating the impact of varying microphysics schemes). Notice that there is little effect in the lower troposphere in terms of PV at this time.

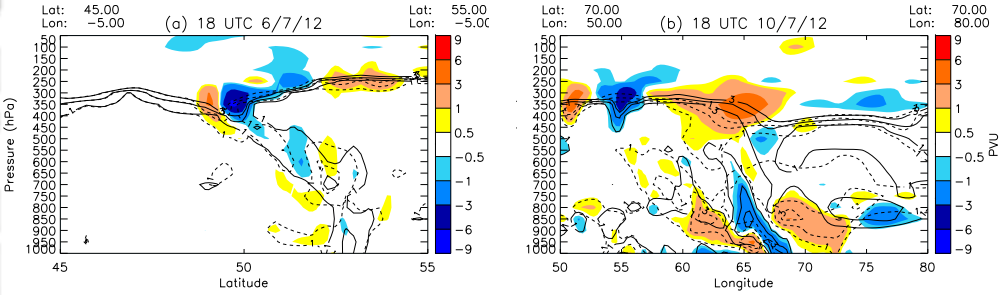

FIGURE 10 Vertical cross-sections of differences in PV (ALLPERTS minus Control) at (a) one day (south–north section) and (b) five days (west–east section) after the MCS perturbations were inserted. Contours of PV (1, 2 and 3 PVU) from the Control output (solid) and ALLPERTS output (dashed) are overlain. The locations of the cross-sections in panels (a) and (b) are indicated on the maps shown in Figs 8(d) and 13(a), respectively.

The MCS perturbations lead to synoptic-scale differences in PV, windspeed, Z and PMSL downstream from the initial MCSs at medium-range forecasting timescales. Figure 11 shows the PV250 (top row) and PMSL (bottom row) differences arising from the addition of the ALLPERTS perturbations after two and three days for a domain spanning most of the northern hemisphere. The PV250 differences are collocated with the tropopause-level ridge and trough pattern around the position of the MCSs and somewhat downstream (as can be seen from the overlain contours of PV250 from the Control simulation). While initially the PV250 differences were localised to the region where the perturbations were added (Fig. 8(c)), these spread upscale into a wider area that is mainly downstream of the initial location as the simulation progresses and within five days both positive and negative differences are observed throughout the northern hemisphere (Fig. 11(a, b) and Fig. 12(a)). This rapid upscale difference growth is consistent with the finding of Stensrud (1996) that Z differences attributable to MCSs can extend longitudinally across a quarter of the hemisphere after 96 h (from comparing model simulations with and without latent heating). However, these differences have their largest amplitude along the tropopause boundary in the ridge over central–eastern Europe (between 10 and 80°E), immediately downstream of where the MCS perturbations were inserted. Upper-level differences in PV and Z due to variations in diabatic heating have been shown to amplify and spread downstream from an initially very localised area in previous studies (Schäfler and Harnisch, 2015; Joos and Forbes, 2016; Grams and Archambault, 2016). The dipoles of PMSL produced in Fig. 11(c, d) show similarities to Fig. 1 of Joos and Forbes (2016). These authors state that the the dipole structure is a balanced response to the PV differences created at upper levels, but noted that not all PMSL differences would be attributable to the differences in upper-level PV.

The predominantly negative PV250 differences (exceeding 3 PVU in magnitude) in this ridge region implies that the MCS perturbations have led to a strengthening and northwards movement of the ridge. The PMSL differences created (Fig. 11(c, d)) spread upscale more slowly than the PV differences. After two and three days differences exceeding

0.5 hPa are found along tight pressure gradients and in the vicinity of low pressure centres directly beneath (and so influenced by) the cyclonically wrapping up PV250 filament. As will be discussed in Section 6, by five days the largest magnitude differences in PMSL (exceeding 3 hPa) due to the ALLPERTS perturbations occur as a dipole associated with a low pressure system located over northern Russia (at about 70°N, 70°E). Negative differences occur to the northwest of the low centre in the Control simulation implying that the MCS perturbations have shifted the system northwestwards. A west–east vertical cross-section of PV difference through the location of this system (Fig. 10(b)) shows that the displacement of the low pressure centre due to the MCS perturbations has an associated westwards displacement of the lower-tropospheric slantwards-tilting positive PV anomalies together with large tropopause-level differences in PV but small midtropospheric PV differences. This impact of the MCS perturbations on lower-tropospheric levels five days after MCS perturbation insertion can be contrasted with the lack of such an impact after one day (Fig. 10(a)); both cross-sections are through cyclonic regions although they differ in orientation and the length of the section shown is much longer at five days. Large tropopause-level impacts are found at both times. The lower-tropospheric changes are consistent with the expected coupling between the upper and lower levels due to baroclinic development and are likely amplified by diabatic processes in the ascending warm conveyor belt of the system.

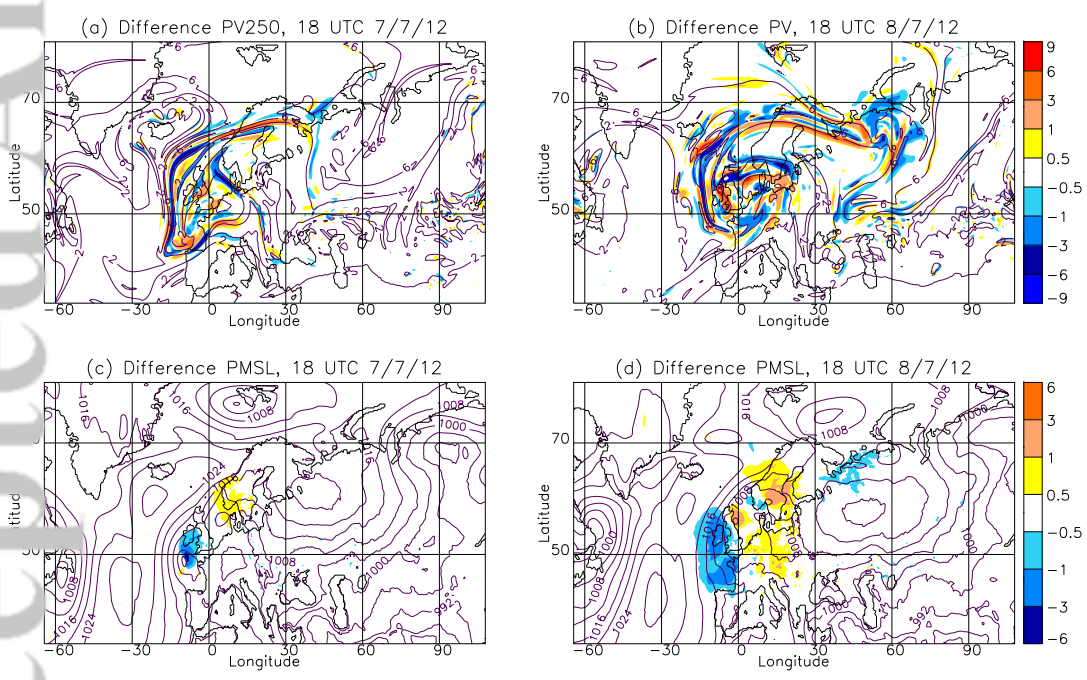

FIGURE 11 (a,b) Differences in PV250 (ALLPERTS minus Control) at (a) two days and (b) three days after the MCS perturbations were inserted. Contours of PV250 (in PVU) from the Control output are overlain. (c,d) As for (a,b), but for PMSL (in hPa).

6 | DOWNSTREAM INFLUENCE OF MCS PERTURBATIONS: DEPENDENCE ON PERTURBATION TYPE

The impact of the MCS perturbations is dependent on the level where they were inserted and their magnitude. Figure 12 shows the PV difference fields after five days for the ALLPERTS, UPERTS, X3PERTS and MPERTS perturbations. The location of the largest amplitude differences are similar for all four perturbation types, lying mainly along the central European ridge. However, although the amplitudes of the differences are larger for the ALLPERTS perturbations than for either the UPERTS or MPERTS simulations (as expected), they are far larger for the UPERTS than for the MPERTS perturbations (compare Figs. 12(b) and (c)). The differences for the X3PERTS perturbations have larger amplitude and are more extensive than for the UPERTS perturbations (compare Figs. 12(b) and (d)), indicating that poor representation of larger, more intense MCSs would likely have a greater impact on the forecast evolution (i.e. the forecast evolution differences are not saturated for the amplitude of MCS perturbations calculated from the MCSs in this case study).

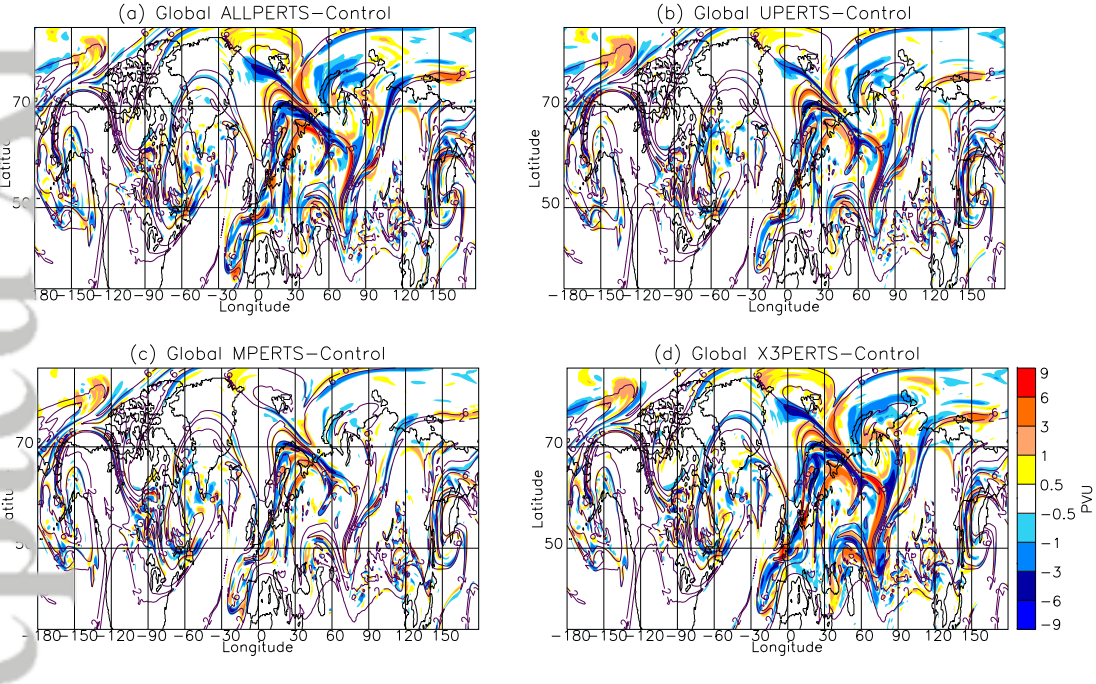

FIGURE 12 Differences in PV250 (with perturbations minus Control) arising from the (a) ALLPERTS, (b) UPERTS, (c) X3PERTS and (d) MPERTS perturbations five days after the MCS perturbations were inserted. Contours of PV250 (1 PVU) from the Control output are overlain.

The greater impact of the UPERTS than MPERTS perturbation is also evident in PMSL. This can be seen for a specific event over northern Russia by looking at the shifts in a low pressure centre from each of the perturbation experiments and is shown in Fig. 13(b). The positions of the low pressure system in the simulations with the other types of perturbations are also shown in this figure. While the MPERTS perturbations have little impact on the system, the system is shifted systematically increasingly northwestwards by the UPERTS, then ALLPERTS and finally X3PERTS perturbations; the central PMSL value is similar in all the simulations. The Met Office analysis valid at this time has a far deeper system to the northeast of those simulated with a central PMSL of 979 hPa. Hence, for this system the

differences between the locations and intensities of the low pressure system in the simulations (with or without the MCS perturbations) are small in comparison to the errors in these simulations compared to the analysis. A poor forecast of this cyclone is not unexpected given the long lead time of this forecast.

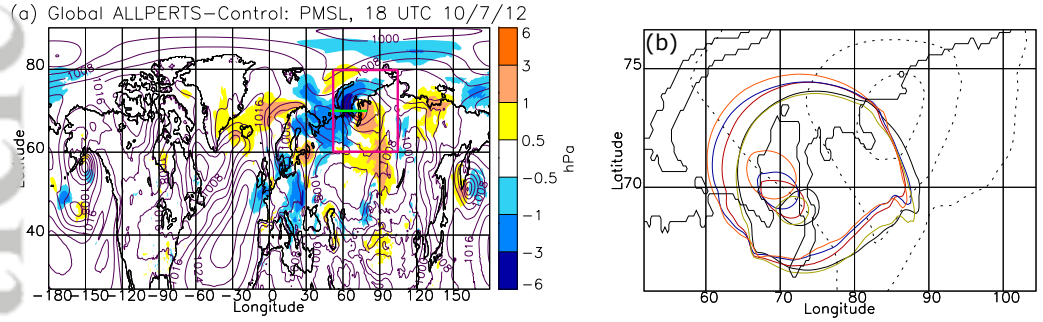

FIGURE 13 (a) Differences in PMSL (ALLPERTS minus Control) with contours of PMSL (in hPa) from Control ...out overlain. The green line indicates the location of the cross-section in Fig. 10(b) and the magenta box the subdomain shown in panel (b). (b) PMSL over northern Russia (contours at 984, 992 and 1000 hPa) for the Global ...lysis (black dotted), Global configuration Control (black) and with MCS perturbations added: ALLPERTS (blue), UPERTS (red), MPERTS (green) and X3PERTS (orange) (a 984 hPa contour is only used for the more intense cyclone in the analysis). Both panels at five days after the MCS perturbations were inserted.

Finally, the RMSD diagnostic has been used to quantify the overall impact of the MCS perturbations on PV250 ... PMSL over the European domain (Fig. 14). The general pattern of RMSD evolution for both fields shows an initial re...uction (or little growth) in amplitude for about 36 h followed by growth that is approximately linear until at least about four days. The growth appears to saturate towards the end of the time period shown, after about four days for PV...50 and possibly in the last 12 h for PMSL. The perturbation experiments with the largest initial RMSD values are ...ose associated with the largest initial reductions in RMSD. This growth evolution suggests that the inserted MCS per...urbations are initially damped by the model, possibly because they have some scales close to the grid scale of the model which are difficult to fully retain (especially if large in magnitude compared to the background variables). As ...ussed previously, the X3PERTS perturbations lead to the largest visual differences in both PV250 and PMSL and this can also be seen in the RMSD diagnostics. At the start of the forecast the RMSD in PV250 due to the UPERTS perturbations is the same as that due to the ALLPERTS perturbations, whereas there is no RMSD due to the MPERTS per...urbations; this is expected because the MPERTS perturbations only extend up to about 450 hPa. Although there is ...initial growth in the PV250 RMSD for the MPERTS perturbations, the RMSD values remain substantially less than those for the UPERTS perturbations at the end of the five-day forecast. This implies that the poor representation of th... anomalously negative PV generated by the MCSs at tropopause level, and the enhancement of the tropopause PV gradient, has more impact on the downstream forecast evolution at tropopause level (and hence Rossby wave ev...ution) than that of the positive PV towers generated in the midtroposphere. This overall greater impact of the UPERTS compared to the MPERTS perturbations doesn't just apply to variables at 250 hPa though, i.e. in the height la...r where the UPERTS were inserted, it also applies to PMSL (Fig. 14(b)). For this field though the RMSD is similar for the UPERTS and MPERTS perturbations for the first 60 hours of the forecast after which the RMSD for the UPERTS perturbations grows far more rapidly than those for the MPERTS perturbations suggesting that the differences in Rossby wave evolution have ultimately led to differences in PMSL and influenced cyclone and anticyclone development.

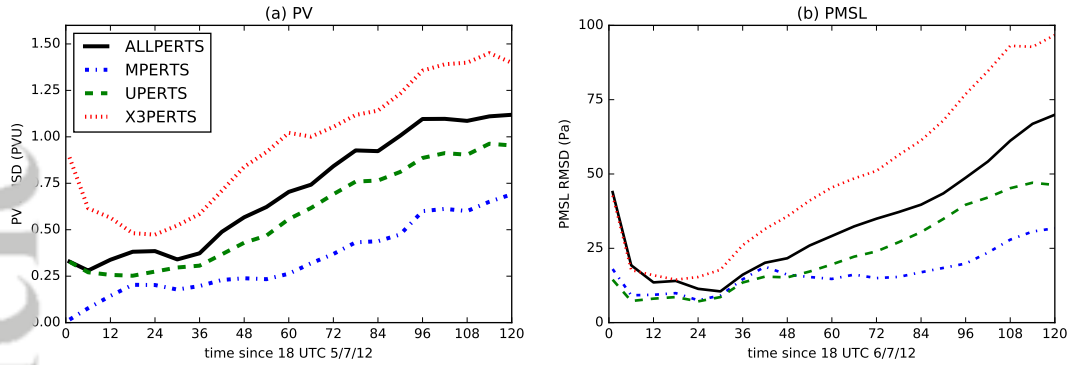

FIGURE 14 Evolution of RMSD (calculated over the European region (30–70°N,-50–100°E)) between the Global configuration simulations with and without MCS perturbations for the four different times of perturbation types for (a) PV250 and (b) PMSL.

7 | CONCLUSIONS

The possible implications of a poor representation of mesoscale convective systems (MCSs) by convection-parametrizing models has been explored here for a single case study using the limited-area convection-permitting (4.4-km grid length) Euro4 and convection-parametrizing (25-km grid length) Global configurations of the MetUM. We first examined the Euro4 and Global model forecasts. We acknowledge that ~4-km grid spacing is not really of sufficiently high resolution to represent individual small thunderstorms, but it is the grid spacing of the model we had available and we argue it does have sufficiently fine resolution to represent MCSs once they have grown to a reasonable size. As expected, the precipitation rates field from the Global configuration simulation of the two MCSs that formed over France (MCS-A and -B, of which MCS-A tracked over the UK) has a smoother structure and smaller values than that from the simulation with the Euro4 configuration. In the Euro4 simulation the MCSs are associated with cores of predominantly positive PV anomalies in the mid-troposphere surrounded by negative PV regions, with more extensive negative PV anomalies (with PV values less than -6 PVU in small regions) at 250 hPa, just below the tropopause. In contrast, there were weak (or no) PV signatures in the Global simulation. The Euro4 PV anomalies associated with MCSs have been shown to be more intense than those in the Global output, even after coarse graining to the same grid spacing. This suggests that the poor representation of the MCSs by convection-parametrizing models can potentially impact synoptic-scale medium-range flow evolution. This hypothesised impact has been tested by perturbing the Global configuration five-day simulations with perturbations of wind and θ (surrogates for PV) derived by calculating the difference between the coarse-grained Euro4 and Global configuration forecasts in the region of the MCSs: so-called MCS perturbations. The impact has been assessed by analysis of the PV at 250 hPa (PV250) (to examine the impact on Rossby waves), as well as surface precipitation and PMSL (to examine the impact on surface weather).

The initial impact (first day) of the MCS perturbations at upper-levels is to modify the extension and depth of an upper-level trough in the geopotential height field associated with a weak surface cyclone that developed over the UK on its eastern flank. The influence of the MCS perturbations extends beyond the region where they are inserted due to the property of PV termed action-at-a-distance. These changes were associated with a better positioning of the cyclone's precipitation and an improved forecast of its PMSL. After five days the differences between the Global simulations with and without the MCS perturbations extend across the entire northern hemisphere. Bands of positive and negative PV differences at 250 hPa mainly lie along the tropopause and are most pronounced around a ridge over

central-eastern Europe that formed downstream of the surface cyclone with which MCS-A interacted, leading to a northwards displacement of the tropopause as expected. The MCS perturbations lead to ridge amplification due to the addition of negative PV anomalies at upper levels. Ridge amplification was also found by Grams and Archambault (2016) when comparing simulations with and without a tropical cyclone included. The effect was of a similar magnitude (PV differences of -7 PVU at 108 h) and covered a similar spatial area to that found here, growing over time (see their Fig. 6). This implies that MCS perturbations can grow upscale to have comparable impacts to those arising from the deep convection within tropical cyclones over medium-range timescales. Similar ridge modifications have also been shown by previous studies that investigated the impact of changing the diabatic heating profile of a warm conveyor belt through reduced humidity (Schäfler and Harnisch, 2015) and altered microphysics (Joos and Forbes, 2016) (both studies used 25 km grid spacing model simulations, the same resolution as used in the Global configuration here) and through running with dry physics (Massacand et al., 2001) (using coarser 0.5° grid spacing model simulations). In Schäfler and Harnisch (2015), reducing the humidity in the initial conditions produced an accompanied reduction in latent heat release and less positive PV was produced at lower levels, a weaker cyclone developed and a lower local tropopause height (by up to 20 hPa) occurred due to the lower outflow height of the warm conveyor belt. In our study the tropopause height was raised by the addition of the MCS perturbations. In Joos and Forbes (2016), varying the microphysics caused no differences in the amplitude of the warm conveyor belt, but caused variations in the positioning of weather systems that led to differences along the leading edge of the warm conveyor belt that spread and amplified downstream similarly to the findings in this study. In Massacand et al. (2001), diabatic heating associated with the upstream cyclogenesis enhanced an upper-tropospheric downstream negative PV anomaly.

The MCS perturbations also lead to changes in PMSL and a north-westwards displacement of a downstream developing surface cyclone (and associated tropopause fold) over northern Russia, implying that the enhanced ridging is associated with slower eastwards Rossby wave propagation. Slowed eastward progression of a synoptic-scale trough was also associated with MCSs in a forecast bust composite by Rodwell et al. (2013) and with tropical cyclones in a composite of such cyclones interacting with extratropical flow by Archambault et al. (2015).

We examined perturbations inserted at different levels and found, unsurprisingly, that MCS perturbations inserted at all model levels at the start of the forecast had more effect on the Rossby wave structure and PMSL after five days than perturbations restricted to only near-tropopause or mid-tropospheric layers. However, the near-tropopause perturbations had substantially more impact than the mid-tropospheric perturbations implying that the negative upper-level PV anomalies generated by the MCSs had more impact on Rossby wave evolution than the positive and negative PV anomalies generated in the mid-troposphere. The near-tropopause PV anomalies impact Rossby wave evolution though their interaction with the pre-existing upper-level trough and its associated tight PV gradient. This interaction likely arises through a combination of a direct PV modification and indirect advection of the PV anomalies by the divergent outflow of the MCSs (as found by Teubler and Riemer (2016) in evaluation of diabatic contributions to Rossby wave evolution, though MCSs were not explicitly considered). The finding that near-tropopause perturbations are most important for the impact appears to contradict Gray (2001) who found from sensitivity studies that the mid-level PV structures of an MCS have the most influence on the downstream flow patterns. However, he inserted idealised PV structures rather than physical structures derived from NWP model data as used here. His idealised PV structure input at near-tropopause levels (centred at 250 hPa) had a minimum magnitude of 0.1 PVU. Here, in contrast, the perturbations added near the tropopause are associated with negative PV values exceeding 3 PVU in magnitude at 250 hPa and so associated anticyclonic circulations rather than the cyclonic circulations that would have been used in Gray (2001).

Finally, the domain-wide RMSDs in PV250 and PMSL between the simulations with and without the MCS perturbations are found to follow a three-stage evolution. For the first 36 h there is typically either a reduction in amplitude

or little growth (dependent on the perturbation experiment and field). The one exception is RMSD in PV250 in the experiment with the mid-tropospheric (MPERTS) perturbations: RMSD grows slowly from zero, as expected because these perturbations are below the 250-hPa level. This initial behaviour is followed by growth for both fields and all perturbation experiments until a tendency towards saturation in the last 12–24 h of the five-day simulations (which happens more quickly in the noisier PV field than in the smoother PMSL field). The initial lack of difference growth suggests that the initially unbalanced winds and θ perturbations are damped by the model. Models that use a convective parametrization scheme have also been shown to underestimate error growth because they are not able to represent rapid error growth on the convective scale (Selz and Craig, 2015a). The MCS perturbations are calculated using Euro4 output coarse-grained to the grid spacing of the Global configuration, whereas the effective resolution of this configuration is somewhat coarser (as described in Sec.4). Hence, another likely cause of the initial damping is that the perturbations have scales that are finer than the effective resolution of the Global configuration and a useful future experiment would be to instead use perturbations generated by coarse graining to the effective resolution of the Global configuration. In time though this damping is overcome by the projection of the perturbations onto growing modes at the synoptic scale. Zhang et al. (2007) identified three stages to error growth (in difference total energy) arising from small amplitude perturbations: growth from small-scale convective instability, a change from convective-scale unbalanced motions to larger-scale balanced motions, and growth of the large-scale components with baroclinic instability (beyond 1 day). Similarly, Selz and Craig (2015b) found rapid initial growth due to convective instability relaxed to large-scale slower growth over about 20 h and Bierdel et al. (2017) demonstrated, using an analytical model, that such relaxation to balanced flow can occur through geostrophic adjustment. Both these studies were with convection-permitting models. However, Zhang et al. (2003) found that initial growth occurred in a convection-parametrizing model associated with nonlinearities in the convective parametrization. In the RMSD diagnostics shown here only the last of these three growth stages is clearly apparent. This is likely a consequence of the PV and PMSL fields considered (which emphasize synoptic-scale differences) and the relatively large amplitudes of the initial perturbations used, though the damping of the initial perturbations is likely associated with the transition from unbalanced initial perturbations to balanced synoptic-scale motions.

Hence, the mis-representation of the PV structures associated with MCSs by convection-parametrizing models to synoptic-scale modification of the downstream flow evolution and so be a potential source of error in convection-parametrizing weather forecasts. The existence of this source of error is consistent with the study by Rodwell et al. (2013) which attributed six-day forecast busts over Europe to MCSs. However, this is the first time, to the authors knowledge, that the possible magnitude and spatial scale of the errors have been demonstrated using MCS perturbations derived from convection-permitting and -parametrizing configurations of the same NWP model. It would be interesting to run a similar experiment for the MCSs represented by a convection-permitting model over the US and examine the downstream effects in the driving global model over western Europe. It is likely these would have a greater effect because the MCSs are wider, deeper and more intense and the North Atlantic storm track is more active and moister than the flow into eastern Europe and Asia. Given that thunderstorm development is inherently unpredictable at small scales in a convection-permitting model, we would not necessarily expect that the approach followed here would produce more accurate downstream forecasts. Instead it provides an alternative plausible trajectory. For that reason it would be more insightful, and practically more useful, to examine this method for an ensemble with the aim of improving the downstream spread rather than correct an individual forecast. This is the subject of the companion paper (Clarke et al., 2019) in which the study presented here is performed using a small ensemble.

8 | ACKNOWLEDGEMENTS

SJC was funded the Natural Environment Research Council studentship 'Multiscale prediction and upscale impact of mesoscale convective systems' (Award reference: 1110110) with a CASE award from the Met Office. We acknowledge the use of the MONSooN system, a collaborative facility supplied under the Joint Weather and Climate Research Programme, which is a strategic partnership between the Met Office and NERC. Operational Met Office analyses, and the initial and boundary condition files needed to run the MetUM simulations on MONsooN, were provided by the Met Office. The data used in this work is available by contacting the corresponding author and is subject to licensing constraints. We acknowledge the interesting questions and helpful comments of two anonymous reviewers.

REFERENCES

Arakawa, A., Jung, J.-H. and Wu, C.-M. (2016) Multiscale modeling of the moist-convective atmosphere. *Meteorological Monographs*, **56**, 16.1–16.17.

Archambault, H. M., Keyser, D., Bosart, L. F., Davis, C. A. and Cordeira, J. M. (2015) A composite perspective of the extratropical flow response to recurving western North Pacific tropical cyclones. *Mon. Wea. Rev.*, **143**, 1122–1141.

Berdel, L., Selz, T. and Craig, G. (2017) Theoretical aspects of upscale error growth through the mesoscales: an analytical model. *Q. J. R. Meteorol. Soc.*, **143**, 3048–3059.

Bloom, S. C., Takacs, L. L., Silva, A. M. D. and Ledvina, D. (1996) Data assimilation using Incremental Analysis Updates. *Mon. Wea. Rev.*, **124**, 1256–1271.

Bowler, N. E., Arribas, A., Mylne, K. R., Robertson, K. B. and Beare, S. E. (2008) The MOGREPS short-range ensemble prediction system. *Q. J. R. Meteorol. Soc.*, **134**, 703–722.

Chagnon, J. and Gray, S. L. (2009) Horizontal potential vorticity dipoles on the convective storm scale. *Q. J. R. Meteorol. Soc.*, **135**, 1392–1408.

Chagnon, J. M. and Gray, S. L. (2015) A diabatically generated potential vorticity structure near the extratropical tropopause in three simulated extratropical cyclones. *Mon. Wea. Rev.*, **143**, 2337–2347.

Chagnon, J. M., Gray, S. L. and Methven, J. (2013) Diabatic processes modifying potential vorticity in a North Atlantic cyclone. *Q. J. R. Meteorol. Soc.*, **139**, 1270–1282.

Clark, P., Roberts, N., Humphrey, L., Ballard, S. P. and Charlton-Perez, C. (2016) Convection-permitting models: A step-change in rainfall forecasting. *Meteorol. Appl.*, **23**, 165–181.

Clark, P. A., Browning, K. A., Forbes, R. M., Morcrette, C. J., Blyth, A. M. and Lean, H. W. (2014) The evolution of an MCS over southern England. Part 2: model simulations and sensitivity to microphysics. *Q. J. R. Meteorol. Soc.*, **140**, 458–479.

Clarke, S. J., Gray, S. L. and Roberts, N. M. (2019) Downstream influence of mesoscale convective systems: Part 2, influence on ensemble forecast skill and spread. *submitted to Q. J. R. Meteorol. Soc.*

Clayton, A. (2012) Incremental analysis update (IAU) scheme. Unifed model documentation paper no.31. *Tech. rep.*, Met Office, FitzRoy Road, Exeter, UK, EX1 3PB.

Davies, T., Cullen, M. J. P., Malcolm, A. J., Mawson, M. H., Staniforth, A., White, A. A. and Wood, N. (2005) A new dynamical core for the Met Office's global and regional modelling of the atmosphere. *Q. J. R. Meteorol. Soc.*, **131**, 1759–1782.

Done, J. M., Craig, G. C., Gray, S. L., Clark, P. A. and Gray, M. E. B. (2006) Mesoscale simulations of organized convection: Importance of convective equilibrium. *Q. J. R. Meteorol. Soc.*, **132**, 737–756.

Grams, C. M. and Archambault, H. M. (2016) The key role of diabatic outflow in amplifying the midlatitude flow: a representative case study of weather systems surrounding western North Pacific extratropical transition. *Mon. Wea. Rev.*, **144**, 3847–3869.

Gray, M. E. B. (2001) The impact of mesoscale convective-system potential vorticity anomalies on numerical-weather-prediction forecasts. *Q. J. R. Meteorol. Soc.*, **127**, 73–88.

Gray, M. E. B. and Marshall, C. (1998) Mesoscale convective systems over the UK, 1981-97. *Weather*, **53**, 388–395.

Gregory, D. and Rowntree, P. R. (1990) A mass-flux convection scheme with representation of cloud ensemble characteristics and stability dependent closure. *Mon. Wea. Rev.*, **118**, 1483–1506.

Harvey, B. J., Methven, J. and Ambaum, M. H. P. (2016) Rossby wave propagation on potential vorticity fronts with finite width. *Journal of Fluid Mechanics*, **794**, 775–797.

Houze, R. A. (2004) Mesoscale Convective Systems. *Rev. Geophys.*, **42**, 43pp.

Joos, H. and Forbes, R. M. (2016) Impact of different ifs microphysics on a warm conveyor belt and the downstream flow evolution. *Q. J. R. Meteorol. Soc.*, **142**, 2727–2739.

Keller, J. H., Grams, C. M., Riemer, M., Archambault, H. M., Bosart, L., Doyle, J. D., Evans, J. L., Galarneau, T. J., Griffin, K., Harr, P. A., Kitabatake, N., McTaggart-Cowan, R., Pantillon, F., Quinting, J. F., Reynolds, C. A., Ritchie, E. A., Torn, R. D. and Zhang, F. (2019) The extratropical transition of tropical cyclones. Part II: Interaction with the midlatitude flow, downstream impacts, and implications for predictability. *Mon. Wea. Rev.*, **147**, 1077–1106.

Lean, H. W., Clark, P. A., Dixon, M., Roberts, N. M., Fitch, A., Forbes, R. and Halliwell, C. (2008) Characteristics of high-resolution versions of the Met Office Unified Model for forecasting convection over the United Kingdom. *Mon. Wea. Rev.*, **136**, 3408–3424.

Lewis, M. W. and Gray, S. L. (2010) Categorisation of synoptic environments associated with mesoscale convective systems over the UK. *Atmos. Res.*, **97**, 194–213.

Liang, A. G. and Fritsch, J. M. (2000) The large-scale environments of the global populations of mesoscale convective complexes. *Mon. Wea. Rev.*, **128**, 2756–2776.

Lillo, S. P. and Parsons, D. B. (2017) Investigating the dynamics of error growth in ECMWF medium-range forecast busts. *Q. J. R. Meteorol. Soc.*, **143**, 1211–1226.

Lock, A. P., Brown, A. R., Bush, M. R., Martin, G. M. and Smith, R. N. B. (2000) A new boundary layer mixing scheme. Part I: Scheme description and single-column model tests. *Mon. Weather. Rev.*, **128**, 3187–3199.

Martínez-Alvarado, O., Madonna, E., Gray, S. L. and Joos, H. (2016) A route to systematic error in forecasts of Rossby waves. *Quart. J. Roy. Meteor. Soc.*, **142**, 196–210.

Massacand, A. C., Wernli, H. and Davies, H. C. (2001) Influence of upstream diabatic heating upon an alpine event of heavy precipitation. *Mon. Wea. Rev.*, **129**, 2822–2828.

McCabe, A., Swinbank, R., Tennant, W. and Lock, A. (2016) Representing model uncertainty in the Met Office convection-permitting ensemble prediction system and its impact on fog forecasting. *Q. J. R. Meteorol. Soc.*, **142**, 2897–2910.

Morris, T. N. (1986) The Spanish plume—testing the forecaster's nerve. *Meteorol. Mag.*, **115**, 349–357.

Roberts, N. M. (2003) The impact of a change to the use of the convection scheme to high-resolution simulations of convective events. forecasting research technical report 407. *Tech. rep.*, Met Office, FitzRoy Road, Exeter, EX1 3PB, United Kingdom. Available from the National Meteorological Library and Archive.

Rodwell, M. J., Magnusson, L., Bauer, P., Betchtold, P., Bonavita, M., Cardinali, C. and Diamantakis, M. (2013) Characteristics of occasional poor medium-range weather forecasts for Europe. *Bull. Amer. Meteor. Soc.*, **94**, 1393–1405.

Schäfler, A. and Harnisch, F. (2015) Impact of the inflow moisture on the evolution of a warm conveyor belt. *Q. J. R. Meteorol. Soc.*, **141**, 299–310.

Selz, T. and Craig, G. C. (2015a) Simulation of upscale error growth with a stochastic convection scheme. *Geophys. Res. Lett.*, **42**, 3056–3062.

— (2015b) Upscale error growth in a high-resolution simulation of a summertime weather event over Europe. *Mon. Wea. Rev.*, **143**, 813–827.

Shutts, G. (2017) Idealized numerical simulations of Mesoscale Convective Systems and their implications for forecast error. *Q. J. R. Meteorol. Soc.*, **143**, 1608–1619.

Stensrud, D. J. (1996) Effects of persistent, midlatitude mesoscale regions of convection on the large-scale environment during the warm season. *J. Atmos. Sci.*, **53**, 3503–3527.

Teubler, F. and Riemer, M. (2016) Dynamics of Rossby wave packets in a quantitative potential vorticity–potential temperature framework. *J. Atmos. Sci.*, **73**, 1063–1081.

Thorncroft, C. D., Hoskins, B. J. and McIntyre, M. E. (1993) Two paradigms of baroclinic-wave life-cycle behaviour. *Q. J. R. Meteorol. Soc.*, **119**, 17–55.

Thorpe, A. J. and Bishop, C. H. (1995) Potential vorticity and the electrostatics analogy: Ertel-Rossby formulation. *Q. J. R. Meteorol. Soc.*, **121**, 1477–1495.

Wandishin, M. S., Stensrud, D. J., Mullen, S. L. and Wicker, L. J. (2008) On the predictability of mesoscale convective systems: Two-dimensional simulations. *Wea. Forecasting*, **23**, 773–785.

— (2010) On the predictability of mesoscale convective systems: Three-dimensional simulations. *Mon. Wea. Rev.*, **138**, 863–885.

Weijenborg, C., Chagnon, J. M., Friederichs, P., Gray, S. L. and Hense, A. (2017) Coherent evolution of potential vorticity anomalies associated with deep moist convection. *Q. J. R. Meteorol. Soc.*, **143**, 1254–1267.

Wilson, D. R. and Ballard, S. P. (1999) A Microphysically based precipitation scheme for the UK Meteorological Office Unified Model. *Q. J. R. Meteorol. Soc.*, **125**, 1607–1636.

Young, M. V. (1995) Severe thunderstorms over south-east England on 24 June 1994: A forecasting perspective. *Weather*, **50**, 250–256.

Zhang, F., Synder, C. and Rotunno, R. (2003) Effects of moist convection on mesoscale predictability. *J. Atmos. Sci*, **60**, 1173–1185.

Zhang, F. C., Bei, N., Rotunno, R., Snyder, C. and Epifanio, C. (2007) Mesoscale predictability of moist baroclinic waves: Convection-permitting experiments and multistage error growth dynamics. *J. Atmos. Sci.*, **64**, 3579–3594.